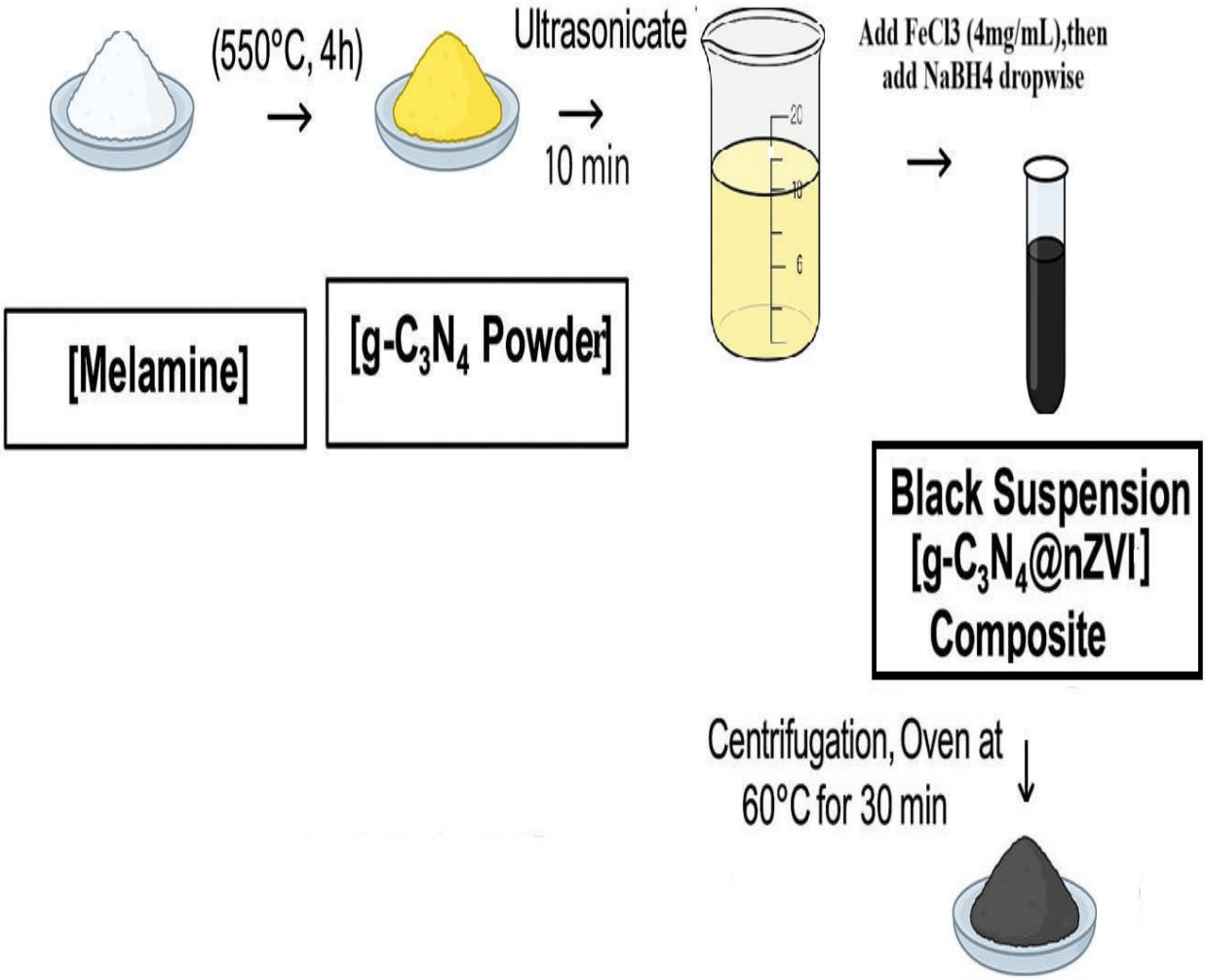

Fig. S1 Schematic representation of the g -C_3N_4@n ZVI synthesis procedure

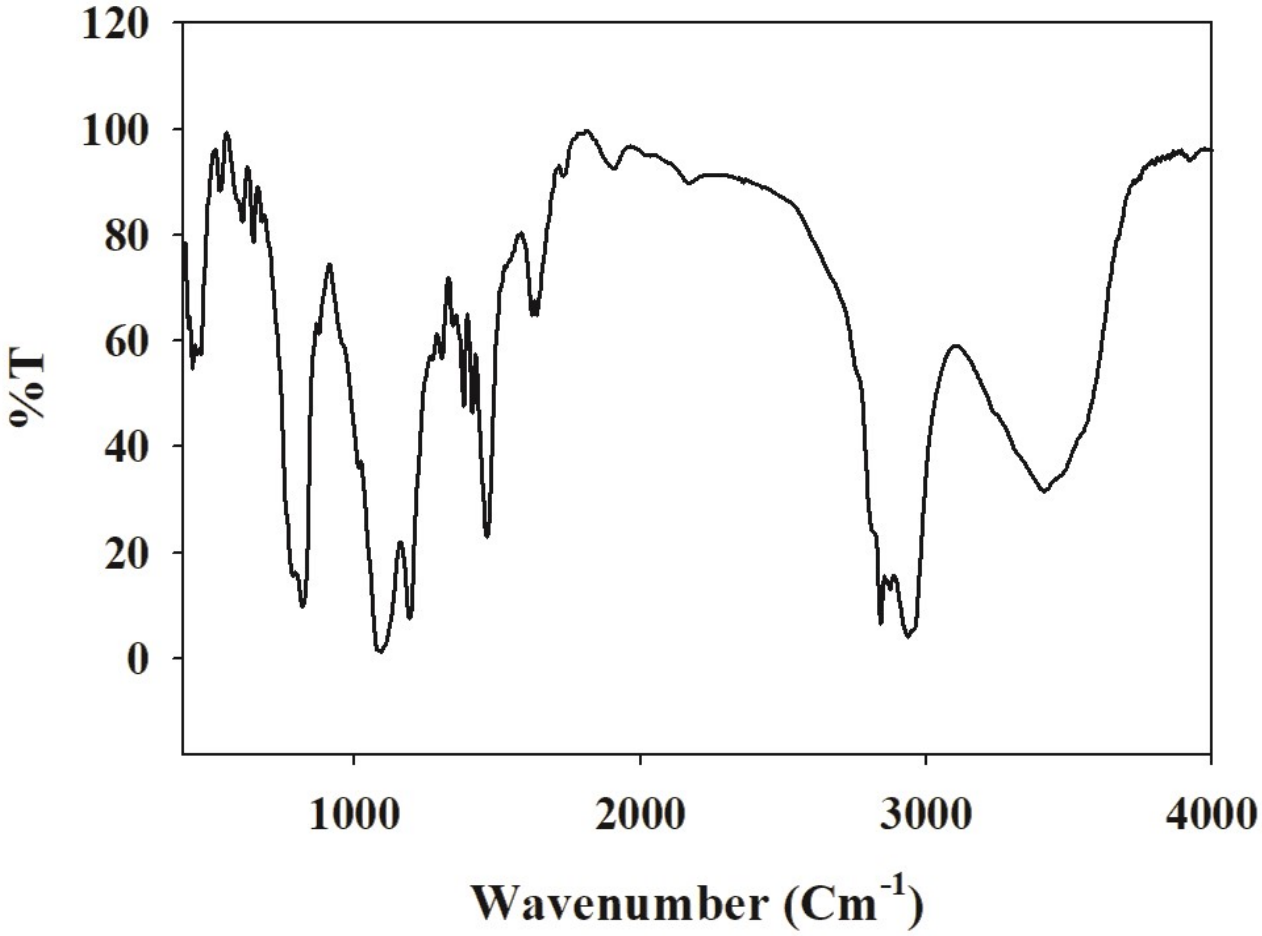

Fig. S2. IR of g -C_3N_4@n ZVI nanocomposite.

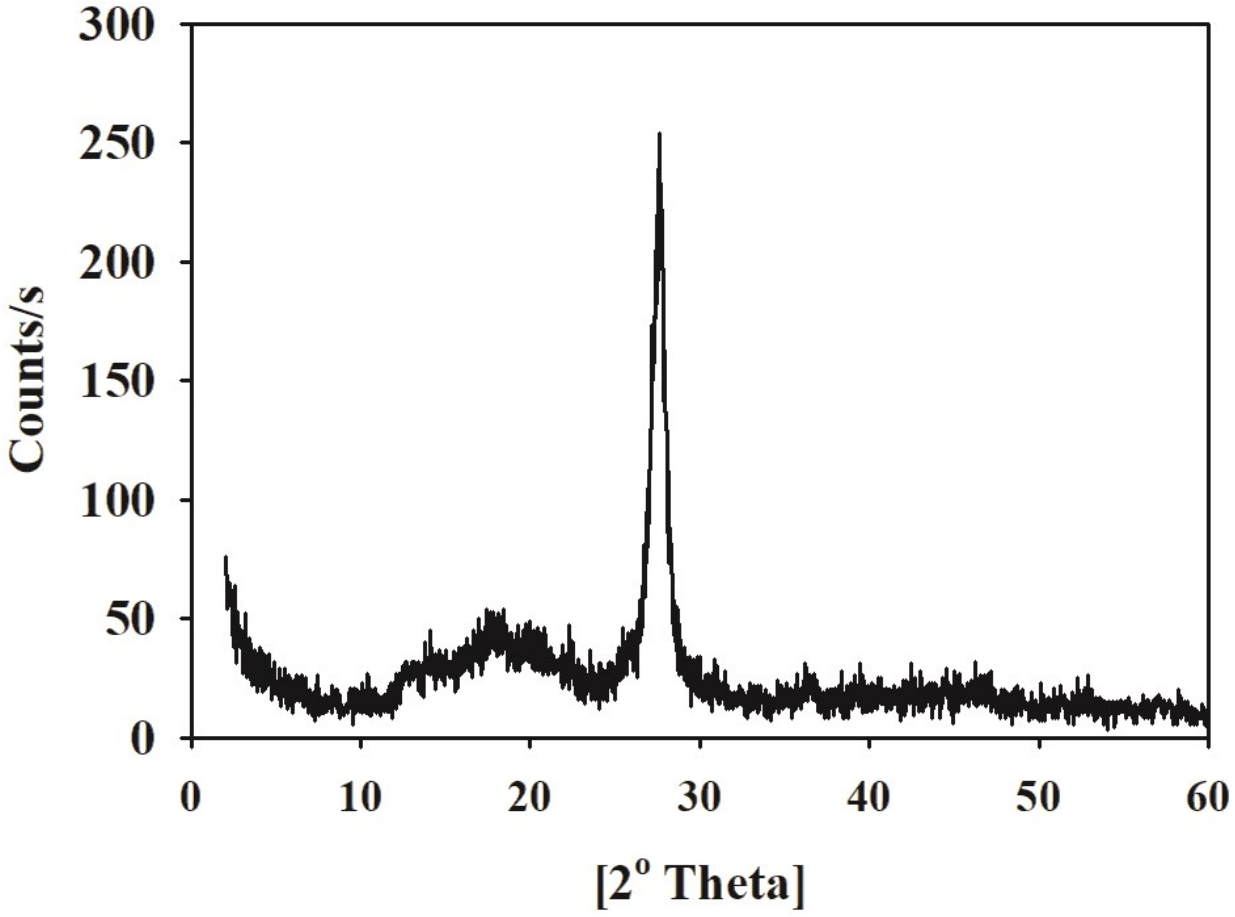

Fig. S3. XRD analysis of g -C_3N_4@n ZVI nanocomposite.

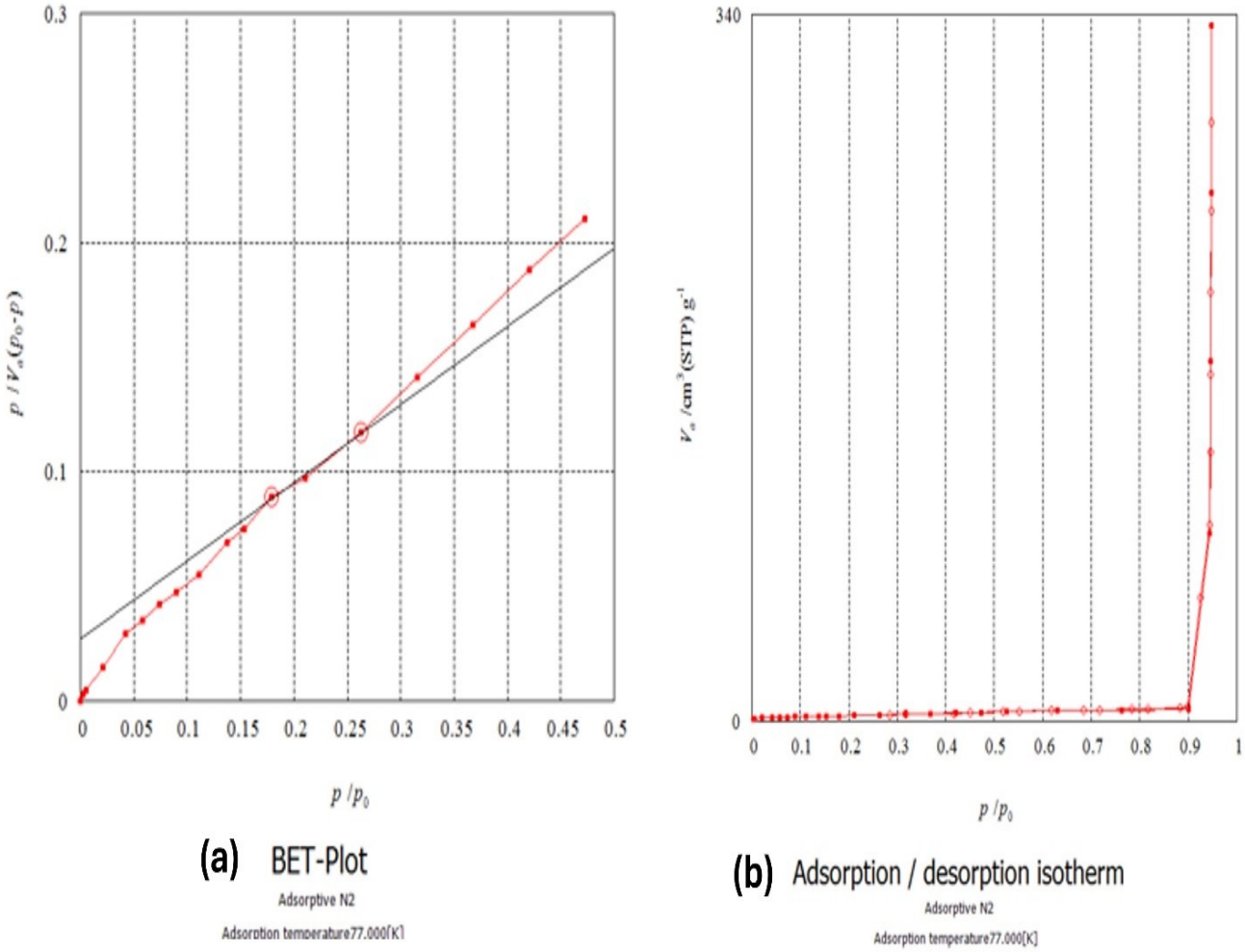

Fig. S4. BET analysis of g -C_3N_4@n ZVI nanocomposite.

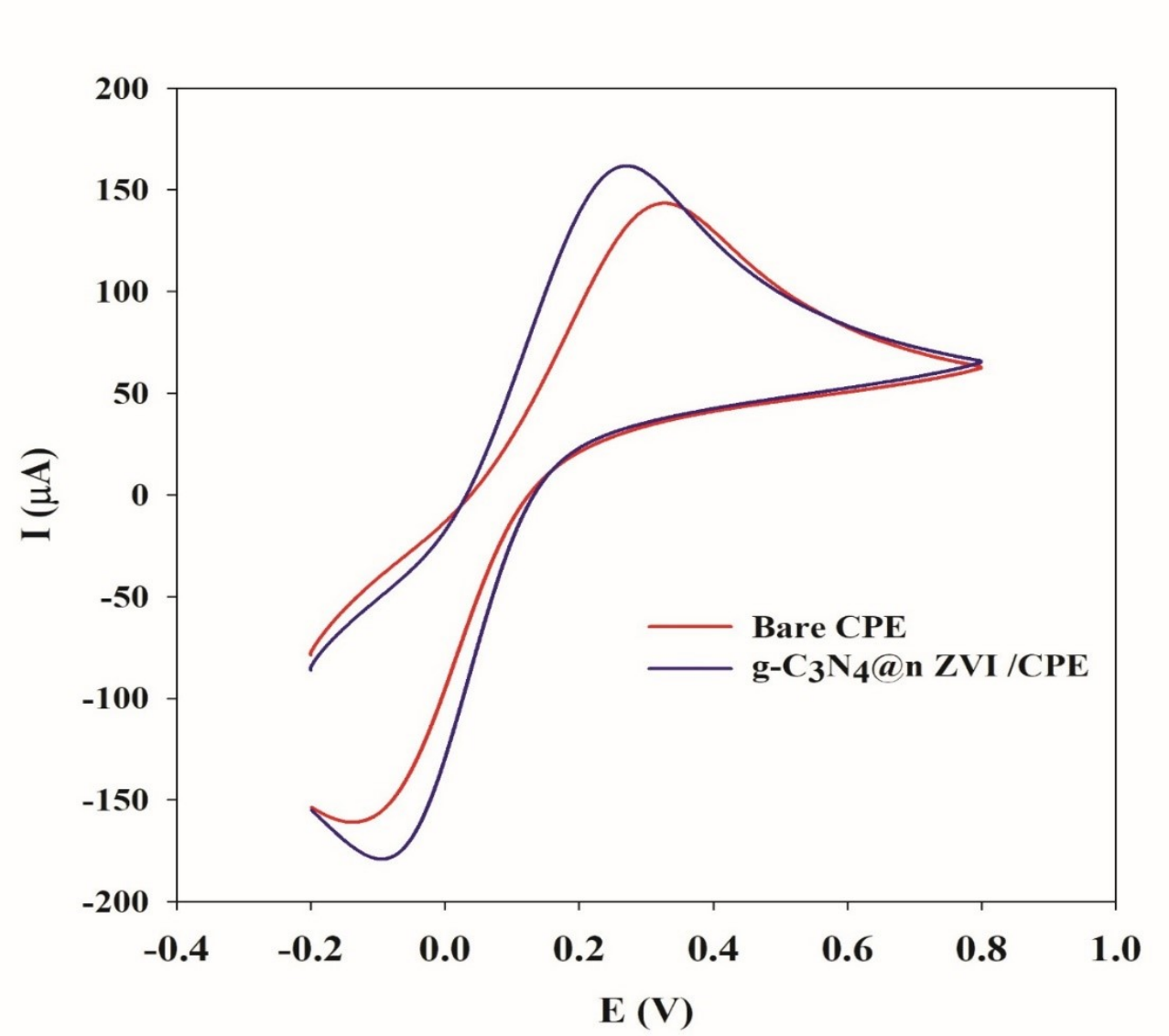

Fig. S5 Cyclic voltammograms of bare CPE and g-C_3N_4@nZVI /CPE in the presence of the 10.0 mM $[Fe(CN)_6]^{3-}$ /$[Fe(CN)_6]^{4-}$ redox system.

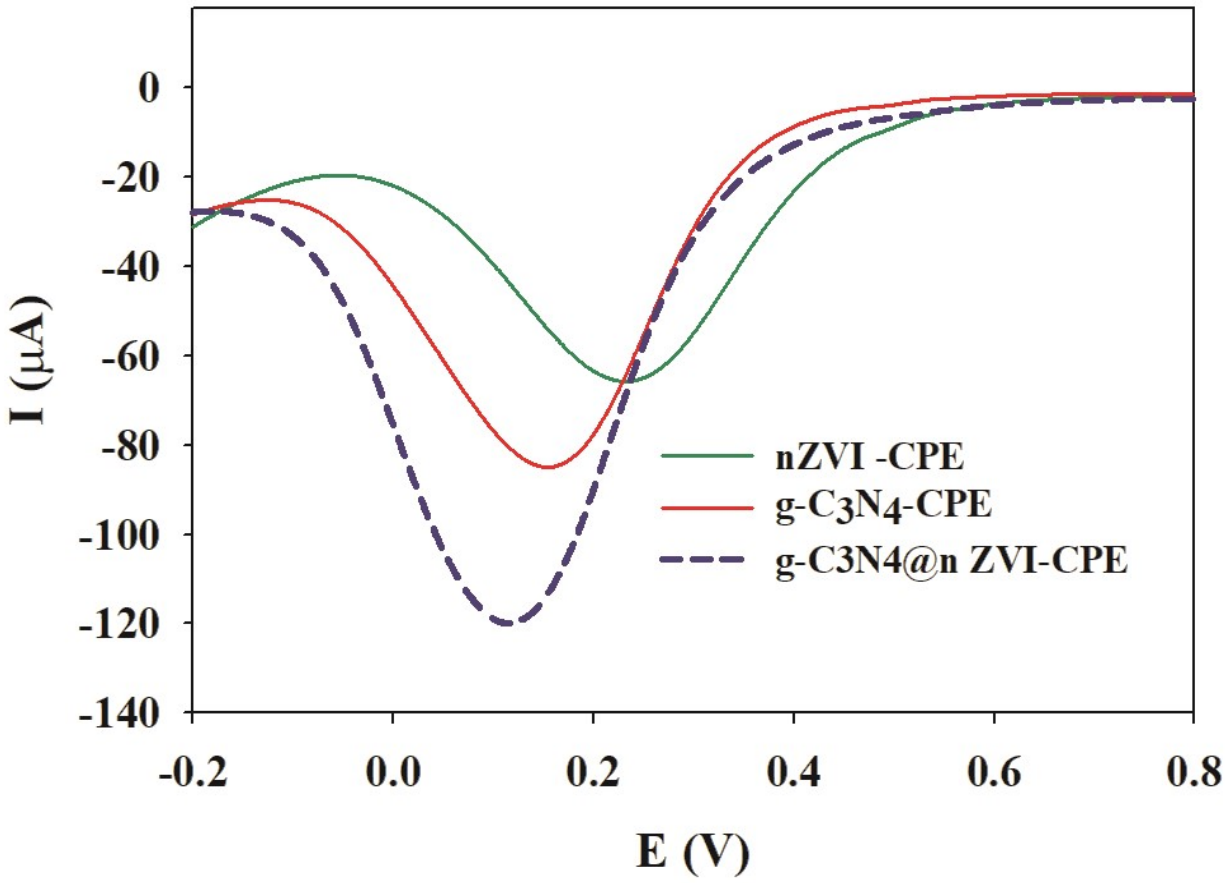

Fig. S6 DPV of potassium ferro/ferricyanide solution (10.0 mM) in PBS buffer at nZVI/CPE, g-C_3N_4/CPE, and g-C_3N_4@nZVI/CPE.

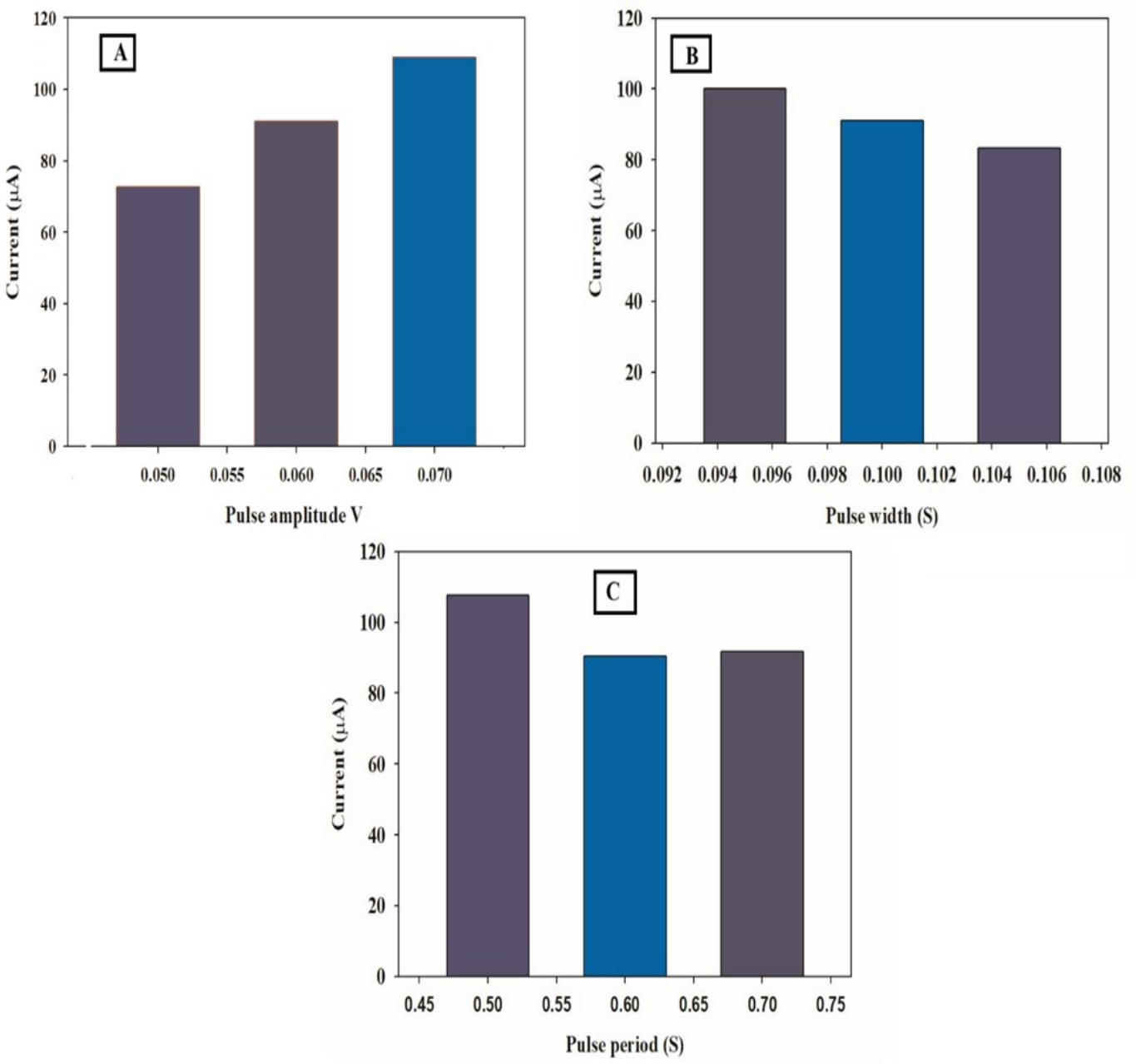

Fig. S7 Optimization of A) Pulse amplitude B) Pulse width C) Pulse period of 1.0 mM HVA in 10 mM PBS (pH = 6) on the g-C_3N_4@nZVI /CPE

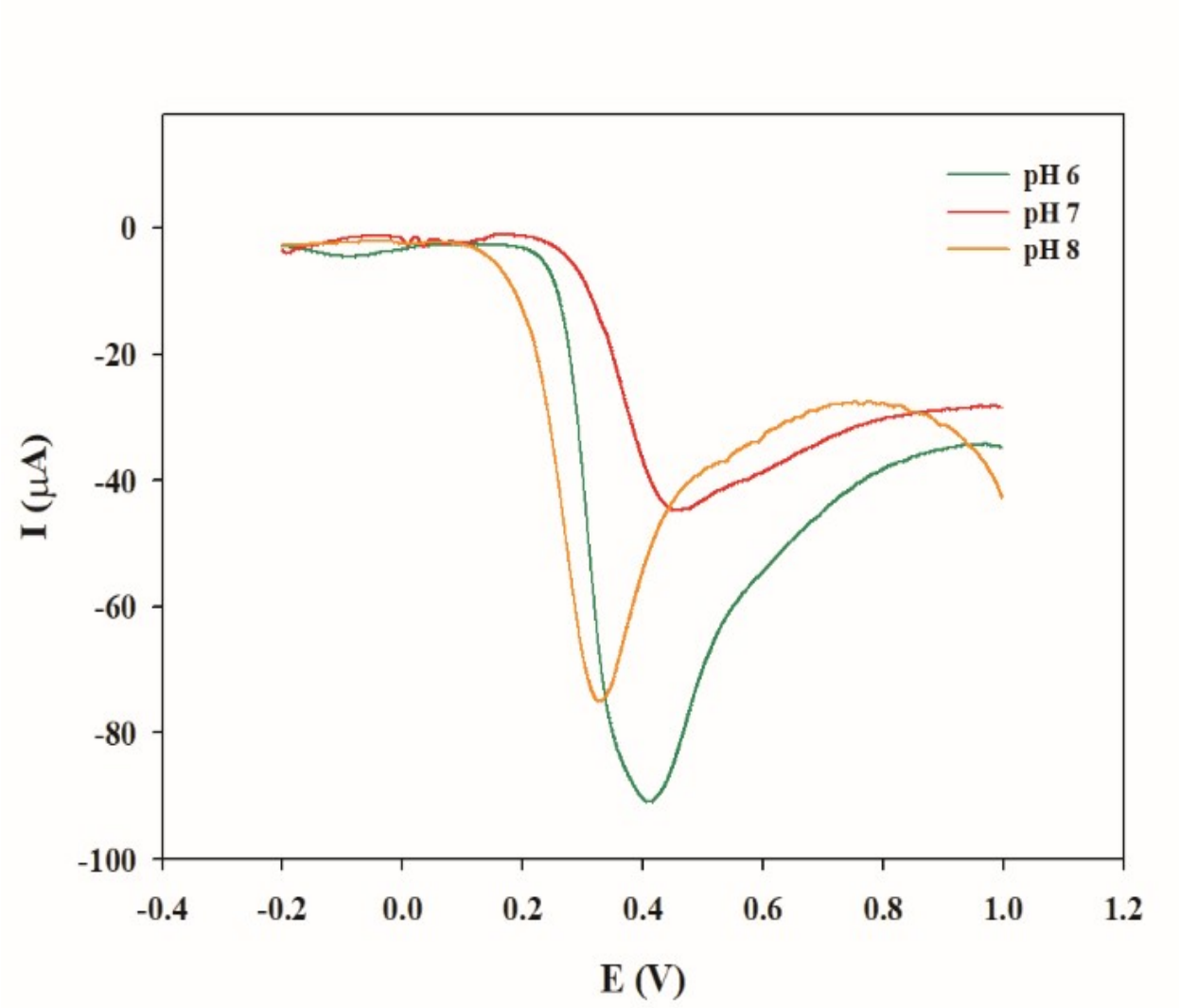

Fig. S8 Effect of pH on the cathodic peak current (Ip).

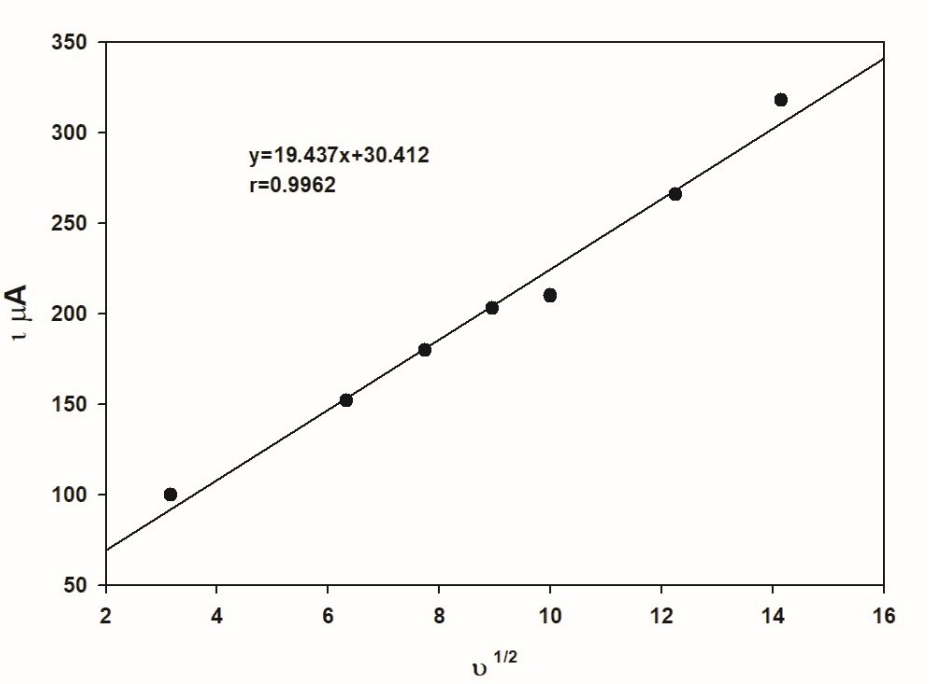

Fig. S9 A plot of the anodic peak current (Ip) of HVA as a function of the square root of scan rate ($\upsilon^{1/2}$).

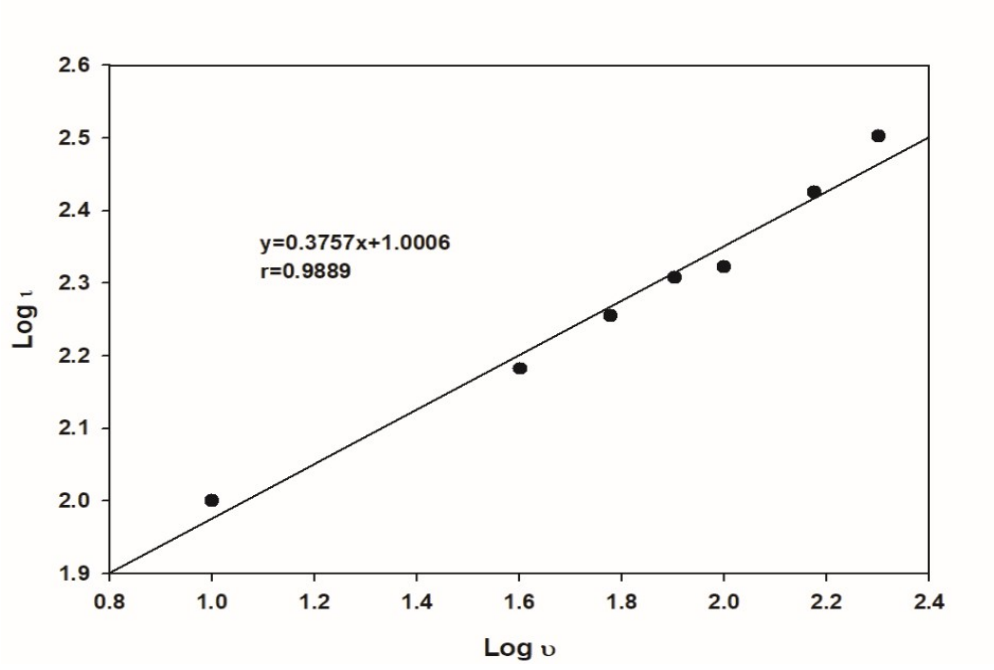

Fig. S10 A plot of logarithm of anodic peak current (log Ip) of HVA as a function of the logarithm of scan rate (log υ) using cyclic voltammetry

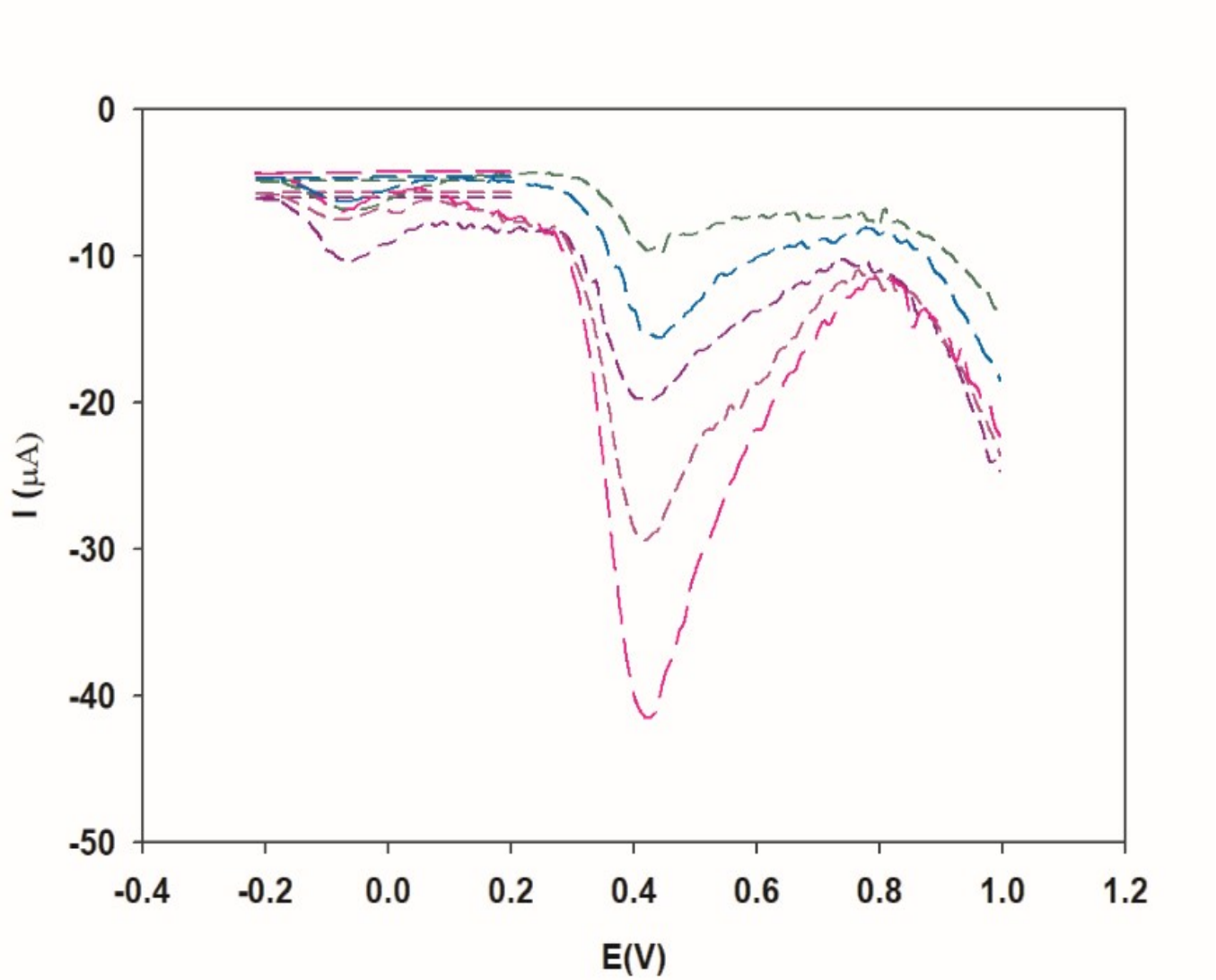

Fig. S11 DPV of different HVA concentrations on the g -C_3N_4@n ZVI /CPE in 0.1 M PBS (pH = 6).